Integrative geochronology calibrates the Middle and Late Stone Ages of Ethiopia's Afar Rift

Elizabeth M. Niespolo[a,b,1,2], Giday WoldeGabriel[c], William K. Hart[d], Paul R. Renne[a,b], Warren D. Sharp[b], M. Steven Shackley[e], Stanley H. Ambrose[f], Berhane Asfaw[g], Yonas Beyene[h], Marianne F. Brasil[b,i], Joshua P. Carlson[i], Yonatan Sahle[j], and Tim D. White[i,k,l,2]

[a]Department of Earth & Planetary Science, University of California, Berkeley, CA 94720; [b]Berkeley Geochronology Center, Berkeley, CA 94709; [c]Private address, Santa Fe, NM 87594; [d]Department of Geology & Environmental Earth Science, Miami University, Oxford, OH 45056; [e]Geoarchaeological XRF Laboratory, Department of Anthropology, University of California, Berkeley, CA 94720; [f]Department of Anthropology, University of Illinois at Urbana–Champaign, Urbana, IL 61801; [g]Rift Valley Research Service, Addis Ababa, Ethiopia; [h]French Center for Ethiopian Studies, Addis Ababa, Ethiopia; [i]Human Evolution Research Center, University of California, Berkeley, CA 94720; [j]Human Evolution Research Institute, Department of Archaeology, University of Cape Town, Rondebosch 7701, South Africa; [k]Centro Nacional de Investigación sobre la Evolución Humana 09002 Burgos, Spain; and [l]Department of Integrative Biology, University of California, Berkeley, CA 94720

Contributed by Tim D. White, October 15, 2021 (sent for review September 3, 2021; reviewed by Shigehiro Kato and Clark Spencer Larsen)

The Halibee member of the Upper Dawaitoli Formation of Ethiopia's Middle Awash study area features a wealth of Middle and Later Stone Age (MSA and LSA) paleoanthropological resources in a succession of Pleistocene sediments. We introduce these artifacts and fossils, and determine their chronostratigraphic placement via a combination of established radioisotopic methods and a recently developed dating method applied to ostrich eggshell (OES). We apply the recently developed ^{230}Th/U burial dating of OES to bridge the temporal gap between radiocarbon (^{14}C) and ^{40}Ar/^{39}Ar ages for the MSA and provide ^{14}C ages to constrain the younger LSA archaeology and fauna to ∼24 to 21.4 ka. Paired ^{14}C and ^{230}Th/U burial ages of OES agree at ∼31 ka for an older LSA locality, validating the newer method, and in turn supporting its application to stratigraphically underlying MSA occurrences previously constrained only by a maximum ^{40}Ar/^{39}Ar age. Associated fauna, flora, and *Homo sapiens* fossils are thereby now fixed between 106 ± 20 ka and 96.4 ± 1.6 ka (all errors 2σ). Additional ^{40}Ar/^{39} results on an underlying tuff refine its age to 158.1 ± 11.0 ka, providing a more precise minimum age for MSA lithic artifacts, fauna, and *H. sapiens* fossils recovered ∼9 m below it. These results demonstrate how chronological control can be obtained in tectonically active and stratigraphically complex settings to precisely calibrate crucial evidence of technological, environmental, and evolutionary changes during the African Middle and Late Pleistocene.

geochronology | Middle Stone Age | Late Stone Age | Middle Awash | Ethiopia

Accurately dating the emergence of *Homo sapiens* and associated technologies in Africa is an enduring challenge in geochronology and a persistent source of frustration for paleoanthropologists (1–3). Most of Africa's Middle Stone Age (MSA) lies beyond the ∼50-ka range of ^{14}C dating, and even Later Stone Age (LSA) occurrences often lack associated charcoal or bone suitable for this technique. Furthermore, crucial Eurasian finds originally dated by ^{14}C have recently required large revisions, highlighting the importance of improved sample preparation even for well-established dating methods (4–6). The ^{40}Ar/^{39}Ar dating of potassium-rich Pleistocene volcanic minerals has yielded solid calibrations based on association and correlation (7–12). However, even when present, many such rocks are contaminated by detrital minerals or lack datable fractions, further limiting application of the technique.

Efforts to overcome these geochronological barriers have often led to adoption of less-reliable techniques such as electron spin resonance, thermoluminescence, or other trapped-charge techniques to obtain varying age estimates for important fossils of emergent *H. sapiens* (refs. 1 and 2, ref. 13 *contra* ref. 14; ref. 15 *contra* ref. 16). Such approaches, often pursued when more tested and cross-validated methods are unavailable, require in situ measurements, may involve questionable assumptions, and/or yield less-precise ages than many radioisotopic decay-based methods (1, 17). Even for more established techniques, methodological developments continue to require revision of earlier chronologies (e.g., ref. 18).

Here we integrate the results of detailed stratigraphic and geomorphological field studies with satellite imagery, tephra chemistry, and multiple radioisotopic chronometers including the recently developed ^{230}Th/U burial dating of ostrich eggshell (OES) (19) to calibrate a suite of stratigraphically superimposed fossil and artifact assemblages from the Middle Awash study area, Afar Rift, Ethiopia. This provides the temporal scale against which ongoing and future studies of key fossils and artifacts will be measured and provides a model approach for other occurrences with similar geochronological challenges and resources. We predict that further applications of this

Significance

Understanding the evolution, dispersals, behaviors, and ecologies of early African *Homo sapiens* requires accurate geochronological placement of fossils and artifacts. We introduce open-air occurrences of such remains in sediments of the Middle Awash study area in Ethiopia. We describe the stratigraphic and depositional contexts of our discoveries and demonstrate the effectiveness of recently developed uranium-series dating of ostrich eggshell at validating and bridging across more traditional radioisotopic methods (^{14}C and ^{40}Ar/^{39}Ar). *Homo sapiens* fossils and associated Middle Stone Age artifacts are placed at >158 and ∼96 ka. Later Stone Age occurrences are dated to ∼21 to 24 ka and ∼31 to 32 ka, firmly dating the upper portion of one of the longest records of human evolution.

Author contributions: E.M.N., G.W., W.D.S., B.A., Y.B., and T.D.W. designed research; E.M.N., G.W., W.K.H., P.R.R., W.D.S., M.S.S., S.H.A., B.A., Y.B., M.F.B., J.P.C., Y.S., and T.D.W. performed research; E.M.N., W.K.H., P.R.R., W.D.S., and T.D.W. contributed new reagents/analytic tools; E.M.N., G.W., W.K.H., P.R.R., W.D.S., M.S.S., S.H.A., B.A., Y.B., M.F.B., J.P.C., Y.S., and T.D.W. analyzed data; and E.M.N. and T.D.W. wrote the paper.

Reviewers: S.K., Hitoto Shizenno Hakubutsukan; and C.S.L., The Ohio State University.

The authors declare no competing interest.

[1]Present address: Division of Geological and Planetary Sciences, California Institute of Technology, Pasadena, CA 91125.

[2]To whom correspondence may be addressed. Email: niespolo@caltech.edu or timwhite@berkeley.edu.

This article contains supporting information online at http://www.pnas.org/lookup/suppl/doi:10.1073/pnas.2116329118/-/DCSupplemental.

Published December 6, 2021.

integrated, basinal-to-submeter geological approach employing multiple geochronological methods will meet ongoing challenges (20) of calibrating and understanding Pleistocene climate change, tectonic processes, environments, technologies, and biological evolution.

The chronostratigraphic framework presented here is foundational to ongoing paleoanthropological studies on a spatially and stratigraphically extensive set of MSA and LSA occurrences in the Dawaitoli Formation of the Middle Awash. We first sketch the history of earlier work and outline our broader stratigraphic findings. We then describe four paleoanthropologically important Halibee member beds. We describe this succession in chronological order, oldest first, summarizing geological and geochronological results and introducing the paleoanthropological content of each. The broader implications of this research are then considered.

Background

The Middle Awash depository of Ethiopia's southwestern Afar Rift comprises variably exposed and tectonically disturbed strata whose cumulative late Miocene through Holocene thickness measures ∼1 km. Paleoanthropological work in the 1970s by Kalb et al. (21) was followed by our Middle Awash research project that began in 1981. We have recovered hominid fossils from 14 separate time-successive horizons, cataloged 33,803 vertebrate fossils from 431 localities, established 69 excavations within 311 archaeological localities, and procured ∼2,000 geological samples. These resources are now broadly chronologically calibrated across the last 6 My, demonstrating that sedimentation through time in this terrestrial depository was obviously episodic rather than the continuous sequence promoted by the previous project (22).

The Middle Awash study area is geographically divided into artifact- and fossil-bearing areas assigned local Afar names. Localities within them are abbreviated with three-letter prefixes (e.g., HAL-A1). Thus, the term "Halibee" applies equally to a village, a wadi, and to the Halibee member geological unit (23, 24). Middle Awash deposits contain an array of archaeological occurrences ranging from Oldowan to LSA, but research has historically focused on rich and extensive Acheulean occurrences (21). Establishment of chronostratigraphic and spatial control over the area's MSA and LSA resources proved more difficult, requiring extensive field and laboratory research and methodological advancements of the last two decades.

For example, the area's best-known MSA assemblages were first recorded in the 1970s and became the focus of intense work in the Aduma area during the 1990s (3, 21, 25). Precise geochronological placement proved elusive because various methods were only able to calibrate the younger Aduma MSA at roughly 80 to 100 ka, whereas the underlying Aduma MSA assemblages (ADU-A1) were not dated.

The LSA of the Middle Awash was first recorded in "Holocene" beds near the Namey Koma hills in the headwaters of the Messalou wadi, a tributary of the Awash River (Fig. 1) (21). Clark et al. (26) confirmed LSA occurrences in the Oulen Dorwa (OUD) basin in stratified sections that remained undated until now. Results presented here provide ages for the Middle Awash MSA and LSA that reveal occupation of the Afar Rift floor before and during the Last Glacial Maximum (∼26 to 19 ka) (27), contemporaneous with human occupation recently documented from southwestern Ethiopia (28) to central Tanzania (29).

As a result of our ongoing research, MSA and LSA occurrences have now been documented as widely distributed across the Middle Awash study area. The richest, least disturbed, and most spatially and stratigraphically extensive of them lie within a deep stratified section best exposed in largely unvegetated erosional topographies in catchments of the Kada and Ounda Halibee western tributaries of the Awash River (Fig. 1). The LSA is embedded near the top of the stratigraphic succession in sediments that overlie strata containing the progressively older MSA and Acheulean assemblages (*SI Appendix*, Figs. S1–S7).

Adjacent, penecontemporaneous deposits north of the Middle Awash study area present analogous challenges to calibrating their paleoanthropological resources (30, 31). These include limitations of radioisotopic dating, rapid facies changes, and syndepositional faulting in a dynamic geomorphic setting. Careful establishment of faults, slumps, inverted channels, erosional features, useful marker horizons, and volcanic strata related to fossils and artifacts are keys to successful stratigraphic placement, and this work is underpinned by strong field logistics and iterative laboratory studies. In keeping with the Middle Awash project's long-term scientific, development, and resource management goals (32), the challenges of creating an adequate chronostratigraphic framework for the Pleistocene artifacts and fossils were met by the integrative approach to chronostratigraphy presented here.

Results

Dawaitoli Formation. The steep gradient of the modern Awash River north of its Messalou confluence (Fig. 1) results in active downcutting, a northerly narrowing riverine forest and floodplain, and active headward erosion into the primarily fluvial sediments comprising the flanking Plio-Pleistocene Dawaitoli Formation (24). Today, the main Awash tributaries (Messalou on the east and Wallia, Halibee, and Talalak on the west; Fig. 1) further expose extensive sediments for a north-to-south distance of ∼25 km in the northern sector of the Middle Awash study area. The Dawaitoli Formation's youngest strata lie ∼90 m above and west of the modern Awash River in the Halibee area. The overall succession dips slightly to the west, its sediments ranging from Holocene to Pleistocene, sampling the last ∼700 ka.

Understanding the complex and dynamic erosional/depositional interfaces that operated here during the Pleistocene was key to the Halibee chronological framework presented below. Fluvial deposition and erosion through time was largely controlled by the base level of downstream depocenters as the northward-flowing axial Awash River was tectonically dropped and/or volcanically dammed by the ongoing extension-related tectono-volcanic activity of the Afar Rift. These erratic tectonic and geomorphological conditions pertain even today in the Middle Awash, with tributaries such as the Kada Halibee seasonal stream featuring rapid headward erosion that broadly exposes the Dawaitoli Formation's sediment stack. In contrast, lower gradient stretches of the Awash River in the southern sector of the Middle Awash exhibit broad floodplains, lakes, swamps, and riverine forest and currently feature active sedimentation (Fig. 1). The utility of these modern analog settings in the inference of Pleistocene depositional and occupational conditions is discussed below.

Artifacts and fossils of the Dawaitoli Formation were embedded in this dynamic setting in which sedimentation was influenced by abrupt tectonic and consequent geomorphological changes. The result was a time-transgressive, shifting interface between erosion and deposition, all with climatic variation proceeding independently. Modern erosion today exposes the Formation's deposits on a broad scale (Fig. 1). The current lack of vegetation cover allows excellent visualization and even remote tracing of stratigraphically superimposed lithological units via satellite imagery. Combining these data with ground-truth investigation has revealed recurrent cut-and-fill features, including inverted paleotopography evidenced by inverted fluvial channels

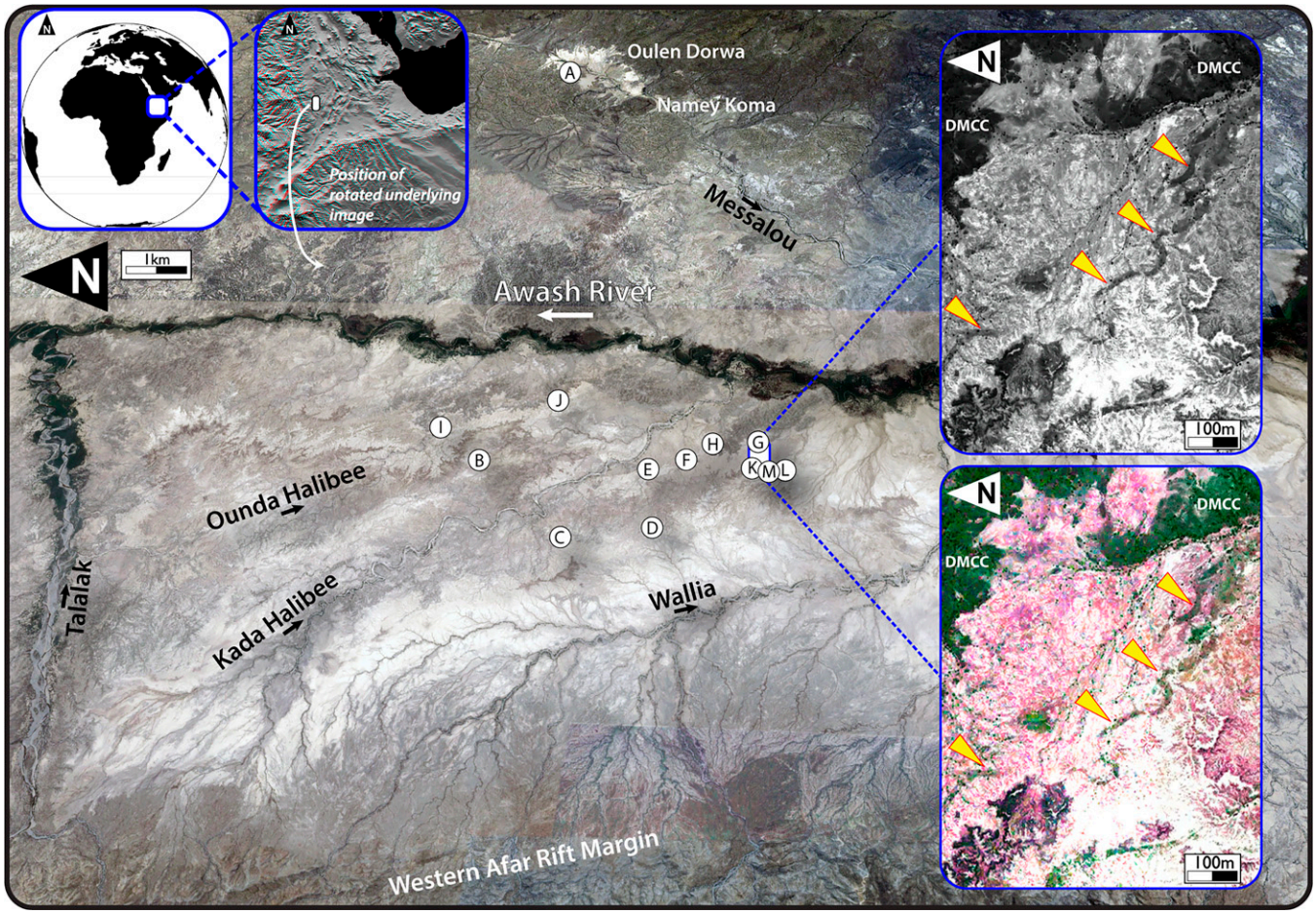

Fig. 1. Satellite imagery of the northern sector of the Middle Awash study area at synoptic and precision scales. Base image is a three-dimensional perspective view to the east from above the western margin of the Afar Rift. White lettered circles mark the lettered sections in Fig. 2. *Inset* imagery is panchromatic and multispectral Worldview-2 imagery captured normal to the Faro Daba landscape. Yellow arrows mark the courses of sinuous Pleistocene paleochannels currently topographically inverting due to local erosion. Fossiliferous ~100-ka Faro Daba beds were emplaced north and east of these channels directly atop darker surfaces of the DMCC that had been locally reexposed by paleo-erosion that removed the older Chai Baro beds. The ~158-ka DGST of these beds is the most reflective sediment in the lower right corner of the insets. See *SI Appendix* for details and illustrative ground-truth photographs.

that parallel those documented for Utah, Egypt, Australia, and China (see refs. 33 and 34 for reviews) and even Mars (35, 36) (Fig. 1 and *SI Appendix*, Figs. S8–S10).

Halibee Member Stratigraphy. The MSA and LSA occurrences described below derive from the Halibee geological member, informally recognized here, and were deposited during the late Middle and Late Pleistocene. The member is informally divided (from the base upward) into four sedimentary beds: Chai Baro (MSA), Faro Daba (MSA), Wallia (LSA), and OUD (LSA) (Fig. 2). Outcrops of the first three beds lie in the Halibee (HAL) region, ~15 km west of counterparts in the small OUD sedimentary basin perched east of Namey Koma in the headwaters of the Messalou wadi (Fig. 1).

Halibee member sediments are primarily associated with the Pleistocene paleo-Awash River and its tributaries. Sediments range from fine-grained silts and clays to sands, interbedded tephra, and massive cobble conglomerates derived from the steep Afar Rift escarpment and shoulder to the west. Lithological heterogeneity reflects intense tectonic and fluvial interactions near the western rift margin, as with the penecontemporaneous upper Busidima Formation exposed in the Hadar and Gona study areas to the north (30, 31).

A widespread, usually calcite-cemented, variably indurated, thick (~3.0 to 5.0 m) cobble conglomerate (the Didamela Cobble Conglomerate, DMCC) (*SI Appendix*, Figs. S6 and S7) at the base of the member is a valuable marker horizon. It floors the Chai Baro beds and is traceable for ~8.5 km north to south at roughly the 565 m (southern) to 575 m (northern) elevation. Sourced from the adjacent western rift escarpment and emplaced by high-energy fluvial conditions in a marginal half-graben, the emplacement mechanisms for such thick, laterally extensive conglomerates remain contentious (30, 37, 38). However, their resistance to erosion and often >10 km lateral traceability make some of them useful stratigraphic markers.

Lower depositional energy sediments were abruptly emplaced upon the DMCC. The lowest ~5 m of Chai Baro beds silts and silty clays are richly fossiliferous and contain MSA artifacts. Superimposed on these are ~10 to 15 m of mostly sterile silts, silty clays, and subordinate fine sands, followed by a crucial tephra marker horizon here named the Didale Glass Shard Tuff (DGST). Now precisely dated (below), the DGST is widely present and traceable across the Halibee region. It also serves as a key to understanding the extensive cut-and-fill depositional regime in which the overlying Halibee member MSA and LSA assemblages were emplaced.

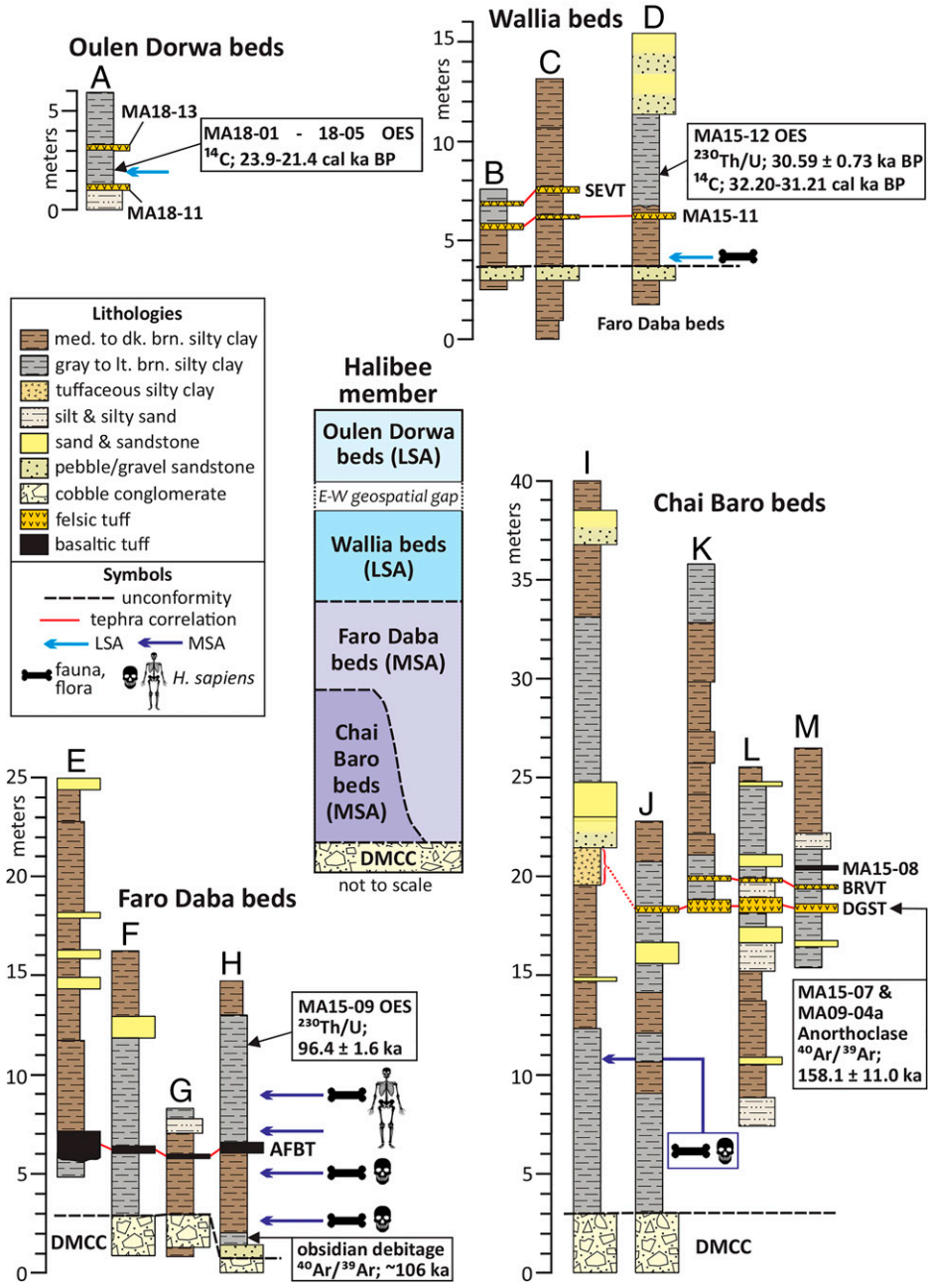

Fig. 2. Halibee member litho- and chronostratigraphy. Measured sections representative of the OUD (*A*), Wallia (*B–D*), Faro Daba (*E–H*), and Chai Baro (*I–M*) beds are illustrated, with letters corresponding to locations plotted in Fig. 1. A central schematic composite section summarizes the relationships between these beds. Important marker horizons and the stratigraphic levels of chronologic results and archaeological and paleontological resources are indicated. Photographs of outcrops on which these sections are based are presented in *SI Appendix*. Descriptions and discussions of the materials and methods used for geochronologic determinations and of the tephra and their chemical signatures are contained in the main text and *SI Appendix*. A more detailed presentation of the age determinations is summarized in Fig. 3.

Following additional relatively low-energy deposition, paleoerosion locally removed substantial thicknesses of the Chai Baro beds across a wide swath of the Halibee region. This erosional downcutting sometimes reached and reexposed the resistant DMCC and is today best evidenced as inverted channels (*SI Appendix*, Figs. S8–S11). Such channeling contributed to the undulating paleotopography atop the DMCC. In an area near the Faro Daba village, one such channel is obvious in satellite imagery as a meandering feature that laterally truncates the DGST and contains large rip-up clasts of DGST in its bed load (Fig. 1 and *SI Appendix*, Fig. S8). Today these channels are emergent in eroding landscapes of the Halibee member because modern erosion into softer flanking silts leaves the channels topographically inverted. Such paleochannels are today recognizable in the field and satellite imagery by their sand-to-gravel lithologies, and because they now provide better anchorage/drainage for modern *Acacia* bushes than do the soft silty sediments more rapidly eroding from their flanks (Fig. 1, *Insets*).

After the local erosional removal of Chai Baro sediments, the base level for the local paleo-Awash catchment was again relatively elevated. Deposition in the Halibee region then

commenced as the Faro Daba beds were emplaced abruptly and unconformably across the undulating upper surface of the DMCC in places where Chai Baro sediments had been removed. The low-energy sedimentation of the Faro Daba beds' fine-grained overbank and floodplain silts first filled low topography atop the DMCC and eventually submerged it. Abundant fossil wood, burned tree trunks, and carbonate rhizoliths evince relatively dense vegetation spatially and stratigraphically tightly associated with vertebrate fossils and MSA lithics in the several meters of silts and silty clays atop the DMCC. These basal Faro Daba sediments are overlain by a basaltic tuff and a succession of up to ∼15 to 20 m of predominantly silty clays and some fine sands. Atop these are the silty clays, silts, and sands of the now-dated LSA-bearing Wallia beds. The younger, uppermost Halibee member's OUD beds east of the Awash also bear newly dated LSA occurrences.

Below we introduce sedimentological and paleoanthropological contexts and provide tephrochemical and radioisotopic results that constrain the four time-successive sets of paleoanthropological occurrences in the Halibee member.

Halibee's Chai Baro Beds. The richest fossil-bearing deposits in the Chai Baro beds are exposed sinuously and nearly continuously in the Kada and Ounda Halibee catchments over a north-to-south distance of ∼8 km. They are recognized by their silt, fine sand, carbonate components, and buff color that contrasts with the more clay-rich, largely sterile dark brown silty clays with sand lenses that succeed them. The aforementioned DGST is the most prominent and widespread tuff in the Halibee member. Ranging from 0.5 to 1.6 m thick, it is identifiable by its fresh, coarse cuspate and bubble-wall glass shards and occasional pumice clasts. Exposures vary from apparent primary fall deposits to those that have undergone minor reworking. Frequently overlying the DGST is a 5-to-30-cm-thick, dark gray, very fine-grained, bedded and unconsolidated vitric ash, here referred to as the Bartikimber Vitric Tuff (BRVT). Unlike the DGST that has compositionally uniform glass, the BRVT glass preserves a wide linear compositional primary array with secondary compositionally distinct clusters. A compositionally bimodal mafic-felsic tuff is intermittently exposed above the DGST, and less than a meter above the BRVT when present (Fig. 2 and *SI Appendix*, Figs. S21 and S22 and Table S1).

The DGST was the first Halibee member tephra to yield $^{40}Ar/^{39}Ar$ results, an age of 148 ± 34 ka (all errors 2σ or 95% CI, unless otherwise stated) (11). Given the large uncertainty, we resampled the DGST in 2015 (sample MA15-07) from a primary, coarse-grained, fining-upward airfall deposit hosting primary anorthoclase, pumice, and abundant glass shards. Secondary minerals (calcite, anhydrite, and gypsum) were present as well as clays and minor lithics that likely washed or settled in over time. Two size fractions of anorthoclase crystals revealed a population of xenocrystic grains concentrated in the coarse fraction (Fig. 3). Of 44 grains from MA15-07, 32 juvenile grains were combined to yield an inverse isochron age of 159.4 ± 11.6 ka (*SI Appendix*). Whereas the previously published age results from the DGST are less precise than those presented here, we feel that accuracy in such cases is maximized by inclusion of all valid measurements concordant within uncertainty. Thus, we combine all valid data to yield a single weighted mean age; using the inverse variance as the weight factor as is standard practice when combining results with disparate precision. Combined with the previous results, the weighted mean age of the DGST is now 158.1 ± 11.0 ka.

This provides a minimum age for underlying artifacts and fossils in the Chai Baro beds and a maximum age for those in the Faro Daba beds. The Chai Baro *H. sapiens* and other vertebrate fossils and MSA artifacts in locality HAL-VP-5 that lie ∼9 m below the DGST are therefore most probably substantially older than the Upper Herto occurrences ∼60 km to the south (10) because the intervening sediment (Fig. 2 and *SI Appendix*, Fig. S2) is predominantly dark brown silty clays associated with slow or standing water deposition. How much older than Herto remains an open question because more precise chronological placement of Chai Baro has proven elusive given the lack of associated tephra or OES. The use of stratigraphic thicknesses to estimate age in tectonically active and fluviatile zones featuring widely and rapidly varying sedimentation rates is common in modern paleoanthropology despite known challenges in such geologic settings, with only rare, extremely well-dated exceptions (39). We follow ref. 40 in considering simple thickness-based approaches to be ill-founded and potentially misleading in most terrestrial applications. We therefore await further field acquisition of dateable samples to resolve the antiquity of the fossiliferous basal part of the Chai Baro beds.

Abundant vertebrate fossils have been collected from the base of the Chai Baro beds. Lithic artifacts are less abundant than those seen in the younger Faro Daba beds. Excavations have not yet been conducted, pending improved geochronological placement. However, field observations and limited controlled surface collection of one occurrence during paleontological extraction allow initial characterization of the Chai Baro MSA. It shares virtually all technological and raw material attributes with the overlying and younger Faro Daba MSA. Chai Baro flaked stone artifacts include Levallois cores, flakes, and points; retouched points; scrapers; and very large heavy-duty tools (sharpened cobbles). The wide variety of raw material includes lavas, obsidian, and siliceous rocks. Although exposed across fewer square kilometers than the Faro Daba MSA, conjoining lithic sets eroding from fine-grained, rhizolith-rich silts of the Chai Baro beds indicate primary depositional contexts. Available excavatable occurrences are predicted to provide excellent integrity and resolution, *sensu* ref. 41 (*SI Appendix*, Fig. S12).

Fossils from the Chai Baro beds are often well-preserved and sample a rich and diverse terrestrial fauna. Mammalian size range spans from ubiquitous and abundant small mammals up to rhinoceratids, including diverse bovids as well as numerous *Papio* and cercopithecin individuals (*SI Appendix*, Fig. S12). The abundant primates include four hominid specimens, a dentition, femoral fragment, and two partial hominid crania that likely predate the ∼160-ka Herto crania.

Halibee's Faro Daba Beds. The MSA-bearing deposits of the Faro Daba beds were first erroneously called "Issie" (21); incorrect spatial placements on published maps also misidentified the HAL and Wallia tributaries, geographic errors repeated by Negash et al. (42). The Faro Daba beds outcrop most widely atop the undulating platform of the DMCC in the area west of the confluence of the Kada Halibee tributary and the Awash River (Fig. 1). In contrast to the Chai Baro MSA exposed further north, and by fortuitous geomorphological circumstances, Faro Daba's fossiliferous overbank silts and silty clays are widely and horizontally exposed atop the resistant DMCC platform. Geomorphologically, the indurated cobble conglomerate serves as a physical shelf that protects the soft, immediately overlying Faro Daba beds from headward erosion. This has resulted in a low rolling topography that provides uniquely wide windows into the paleolandscape because of the abundant embedded fossils and artifacts concentrated in these relatively soft sediments.

The Faro Daba fossil-bearing sediments across this ∼1.5-km^2 surface contain abundant large rhizoliths at their basal contact with the DMCC and a prominent basaltic tuff marker horizon that usually lies ∼1 to 5 m above the DMCC top (Fig. 2). The paleoanthropological resources of the Faro Daba beds are concentrated above and below this Afcaro Basaltic Tuff (AFBT). It

typically presents as a dark gray to black, unconsolidated to moderately indurated, 5-to-150-cm-thick, fine-sand sized scoriaceous deposit that locally shows evidence of reworking and overthickening in paleochannels. Based on the analysis of five separate samples, the AFBT displays one dominant and one subordinate basaltic glass compositional mode (*SI Appendix*, Figs. S21 and S22 and Table S1).

Abundant fossil wood, burned tree trunks, and rhizoliths evince a biotically rich and temporally brief interval during which the included MSA artifacts and vertebrate fossils were deposited. As with the older occurrences of the Chai Baro beds, the Faro Daba paleoanthropological resources are concentrated in these lower silts and silty clays of the Faro Daba beds, followed by largely unfossiliferous overlying darker silty clays.

Prior work utilized $^{40}Ar/^{39}Ar$ and ^{14}C dating in a series of attempts to constrain the ages of the Faro Daba beds. The Faro Daba remains were emplaced after local erosional removal of the sub-DGST Chai Baro package, and thereby postdate the maximum $^{40}Ar/^{39}Ar$ age of 158.1 ± 11.0 ka for the DGST. Attempts to date the AFBT and the artifacts and fossils interbedded with it have repeatedly failed due to low K concentrations combined with extremely high atmospheric ^{40}Ar concentrations (11). A minimum age of >54 ka (accelerator mass spectrometry ^{14}C-dead) was obtained from charcoal in an in situ burned tree stump charcoal sample (*SI Appendix*, Fig. S7*C*) overlying the AFBT by ∼4 m (11). This result helped to confirm stratigraphic relationships and erosional processes described above, but tighter age constraints were required.

Our original application of $^{40}Ar/^{39}Ar$ to obsidian debitage provided maximum ages for fossils and artifacts at Herto (10), inspiring parallel work on the Faro Daba MSA. We first subjected 21 surface-collected, DGPS (differential Global Positioning System)-controlled obsidian debitage samples to combined X-ray fluorescence analysis, electron probe microanalysis, and $^{40}Ar/^{39}Ar$ age determinations. A chemically and chronologically distinct juvenile population dating to 106 ± 20 ka was identified, thereby constraining the extrusion age of the obsidian and providing a maximum age for the Faro Daba MSA (11).

Building on these results, in 2015 we sampled additional diagnostically MSA surface and in situ obsidian artifacts from the Faro Daba MSA bearing outcrops to assess their chemical compositions and link them with the previously dated obsidians. Of the 17 additional pieces presented here, all were either techno-typologically diagnostically MSA or recovered in situ. Of the 17 pieces, 3 demonstrated major/minor oxide and trace element concentrations that geochemically match the ∼106-ka-dated obsidian (*SI Appendix*, Fig. S27): two bifacial points from HAL-A2 and a retouched flake from the archaeological excavation at HAL-A25 (both Faro Daba beds) (Dataset S1). These obsidians derive from the unknown geological source that was represented by three pieces (MA04-28K, 28O, and 28P) in ref. 11, later characterized as Type 10 in ref. 42. These results exclude the possibility of contamination and conclusively link the ∼106-ka obsidian dates to in situ Faro Daba artifact assemblages, rendering this obsidian extrusion age as the maximum age limit for them.

However, the Faro Daba beds' upper age limit remained constrained only by the infinite ^{14}C age, therefore insufficiently precise for placing the Faro Daba remains. Acquiring a precise minimum age for the Faro Daba MSA required the application of the recently developed $^{230}Th/U$ OES burial dating technique (19). We recovered OES fragments (MA15-09) from ∼5 m above the AFBT (Fig. 2). Numerous OES fragments were collected at a single location, eroding from within a medium to light grayish brown silty clay, likely from a single egg or a larger eggshell fragment, parts of which were excavated in situ. Five fragments were analyzed using laser ablation inductively coupled plasma mass spectrometry (ICP-MS) to characterize the distribution of U and Th in the OES fragments and by solution multicollection ICP-MS to produce $^{230}Th/U$ ages on two subsamples of each OES fragment, yielding 10 $^{230}Th/U$ ages ranging from ∼97 to 91 ka (*SI Appendix*). Three samples produced burial ages consistent with a single stage model of U uptake upon burial (19), yielding a weighted mean age of 96.4 ± 1.6 ka (all errors are 2σ or 95% CI, unless otherwise stated; Fig. 3).

Good agreement of the $^{230}Th/U$ ages among multiple OES fragments indicates that their mean $^{230}Th/U$ age provides a firm minimum age for their hosting stratum. Indeed, close agreement between $^{230}Th/U$ burial ages and ^{14}C ages of younger eggshells observed in this study (see *Halibee's Wallia Beds*) and a prior one (19) shows that OES $^{230}Th/U$ ages may closely date their host strata. Collectively, these relations, along with preservation of stratigraphic order between the mean OES age and the mean age of underlying obsidian, indicates that MSA artifacts and fossils from the Faro Daba beds are now constrained to between ∼96 ka and ∼106 ka.

The lower ∼5 to 10 m of the Faro Daba beds comprise richly fossiliferous silty clays immediately below and above the AFBT. Lithic artifacts accompany the fauna, most concentrated in the average ∼5-m interval between the tuff and the top of the underlying DMCC. Archaeological research began with reconnaissance transects, followed by collection of artifacts derived from sieving operations conducted during fossil recovery, DGPS-controlled surface collections, and, finally, 238 m^2 in five excavations.

Surface and excavated artifacts from the Faro Daba beds closely match, with Levallois cores and products that include points (*SI Appendix*, Figs. S13–S15), technological blades, scrapers, perforators, and other retouched tool types and heavy-duty tools that include core axes and pick forms. Conjoining sets of lithics, often involving many flakes and small debitage, are often found freshly exposed atop the soft eroding silts. Flakes account for more than half of the total artifact count from the excavations. The pooled lithic assemblage is obviously part of the MSA technocomplex in all aspects, including a wide range of raw materials, mostly volcanic rocks probably procured locally from readily accessible clasts in the DMCC, along with imported obsidians and siliceous rocks. Both surface and subsurface artifacts are usually in direct association with faunal remains, primarily rodents and bovids.

A large assemblage of fossil vertebrates has been collected from three major paleontological localities representing the Faro Daba beds (*SI Appendix*, Fig. 16). Because of the striking abundance, integrity, and resolution of the archaeological occurrences sandwiched between the top of the DMCC and the base of the AFBT, initial collection of fauna was restricted to fossils found above the tuff. As in the older Chai Baro silts, the Faro Daba fauna is taxonomically diverse, but proportionally distinct. Rodents are common in the collections, and the bovids range up to eland (*Taurotragus*) size. Primates are remarkably abundant, and many partial skeletons of the dominant cercopithecines and colobines were recovered. Unlike the Chai Baro assemblages, papionins are absent, perhaps indicating Faro Daba's closer proximity to a riverine forest. Included among the primates are an array of 13 cataloged *H. sapiens* comprising a mix of postcranial and craniodental elements. The most complete of these is a partial skeleton, with mandible and cranial vault, of a very large and robust adult, presumed male, individual that eroded from sediments above the AFBT but below the dated OES (sample MA15-09) horizon.

Halibee's Wallia Beds. The Wallia beds comprise the uppermost sediments in the Kada Halibee catchment. Erosion and absence of vegetation allow aerial and satellite imagery to be used as

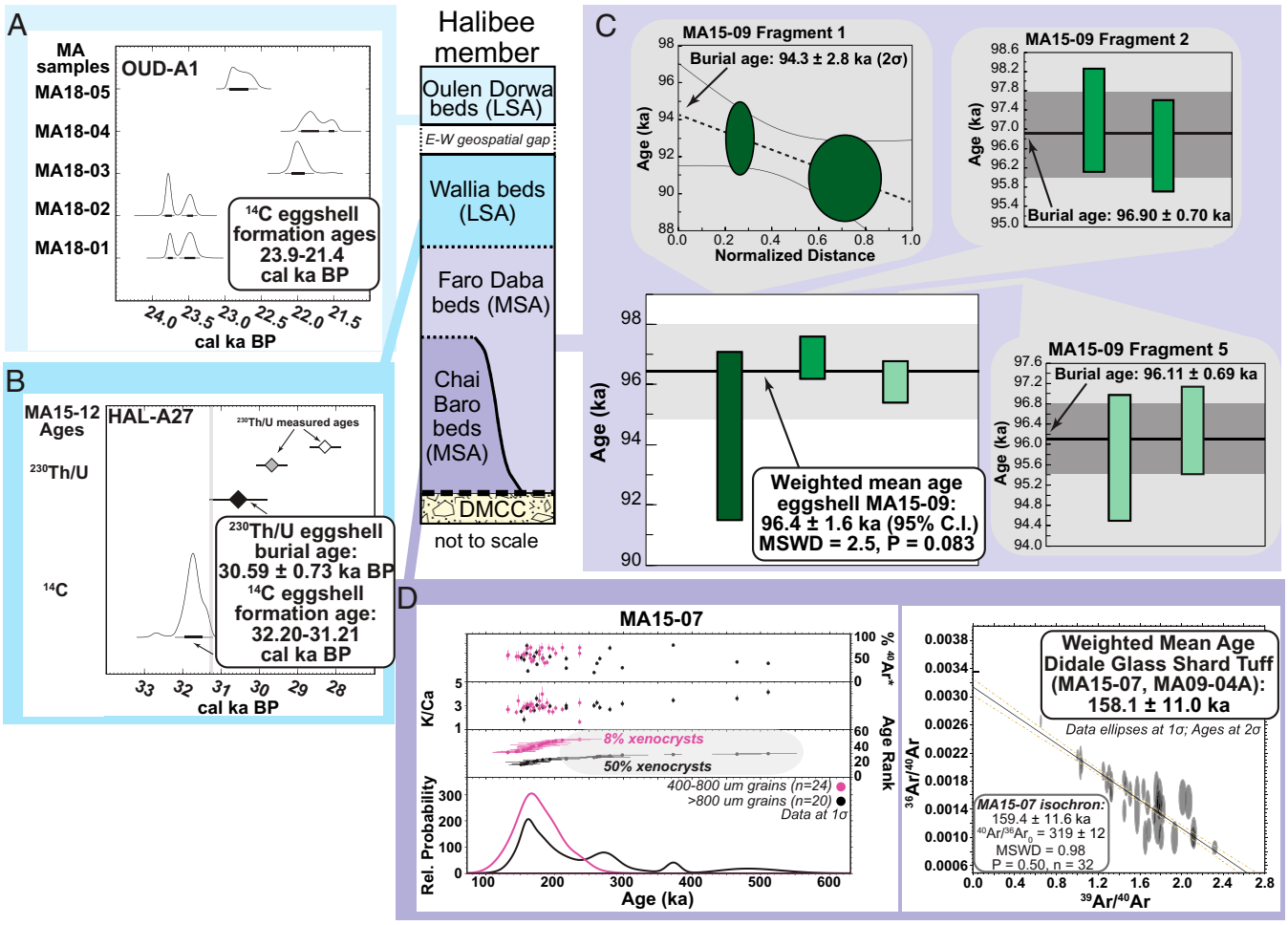

Fig. 3. Radioisotopic ages from the Halibee member; age errors are 2σ or 95% CI. Schematic column (*Center*) shows relative positions of dated samples. (*A*) ^{14}C ages of five OES fragments from locality OUD-A1 in the OUD beds. (*B*) ^{14}C and ^{230}Th/U ages of splits from an OES fragment from locality HAL-A27 in the Wallia beds. (*C*) ^{230}Th/U ages of three OES fragments from sample MA15-09 in the Faro Daba beds; plots for each fragment show measured ages for outer- and inner-shell fractions and resulting burial ages (see *SI Appendix*, section 2.2 for details); remaining plot shows burial ages of each OES fragment and their weighted mean age. (*D*) ^{40}Ar/^{39}Ar data and ages for the DGST. (*Left*) K/Ca ratios (*Upper*), ^{40}Ar/^{39}Ar ages (*Middle*), and relative probability distributions of ages of two size fractions of single anorthoclase grains from sample MA15-07 (*Lower*); shaded areas in middle-left panel indicate grains inferred to be xenocrysts and omitted from the inverse isochron shown in the right panel; note higher xenocryst abundance in coarser grain size. (*Right*) Inverse isochron for anorthoclase grains from MA15-07 after excluding xenocrysts; the final weighted mean age of the DGST (inset age) includes both data from MA15-07 (this study) and from MA09-04 (11). For details, see *SI Appendix* and Dataset S1.

effective mapping tools by which the extent of the Wallia beds can be readily and accurately assessed at large scale (Fig. 1). To date, the Wallia beds are the least investigated Dawaitoli Formation deposits. Limited foot transects across these extensive outcrops included observation and photography of stone tools and fossils eroding from deposits associated with two sampled tephra described below.

The Wallia beds are exposed from at least the southern end of the Wallia catchment northward to the Talalak river, a distance of ∼20 km. Combining our preliminary surveys, tephrochronological results, and imagery, we estimate that many years of intensive foot survey will be required for adequate paleoanthropological survey coverage of these deposits across the ∼50-km^2 exposures. Such reconnaissance is predicted to identify dozens (if not hundreds) of LSA occurrences. Imagery also indicates that these sediments (or their chronological and geomorphological equivalents) stretch far north of the Talalak, to near the Gona wadi where they also include LSA occurrences (30). Here we briefly introduce the Halibee Wallia beds and their contents.

The LSA-associated fossils and artifacts in the Wallia beds uncomformably overlie the Faro Daba MSA and are embedded in light gray to reddish brown silts and medium brown silty clays measuring a total thickness of ∼8 m. These sediments are interbedded with two tephra above a pebble sandstone/conglomerate eroded into underlying dark silts and clays. These tephra are fine-grained, partially reworked, crystal-poor, gray vitric tuffs ranging from 5 to 60 cm in thickness. The lower tuff (MA15-11) was not analyzed, and the upper tuff is represented by three samples spanning a ∼5.5-km north-to-south transect that includes MA15-10. This tuff, the Seegeri Vitric Tuff (SEVT), is compositionally uniform and readily distinguishable from other Halibee member felsic tephra. An additional tuff that is represented by a single isolated sample (MA04-16) has not yet been related to the others but represents a third tephra occurrence in the Wallia beds.

Fragments of a whole, in situ, collapsed ostrich egg (MA15-12; Fig. 2) were extracted from gray, bedded to partially laminated silty clay ∼2 to 3 m above sediments hosting LSA archaeology at locality HAL-A27 in the Wallia beds. Vitric tuff MA15-11 is present between this OES and the archaeology and also outcrops at HAL-A26 1.1 m beneath the SEVT (MA15-10) and atop an analogous LSA assemblage.

This OES find provided an opportunity to further evaluate the fidelity of ^{230}Th/U burial dating by comparing ^{14}C and ^{230}Th/U burial ages on splits of eggshell calcite. Using two measured ^{230}Th/U ages from the OES, we calculated a burial age (after ref. 19) of 30.59 ± 0.73 ka BP. This age overlaps, albeit slightly, with the 95% CI of the ^{14}C age [32.20 to 31.21 cal ka BP (43, 44); Fig. 3 and *SI Appendix*]. The ^{14}C age dates eggshell mineralization, and the ^{230}Th/U burial age dates initial contact of the eggshell with U-bearing soil water. Overlap between the two results indicates OES burial and U uptake ensued shortly after eggshell mineralization, i.e., within the analytical uncertainties of the two techniques. The Wallia LSA is therefore dated to ∼31 ka based on the mutually consistent ^{14}C and ^{230}Th/U burial OES ages.

The two archaeological localities thus far established in the Wallia beds were created to document the presence of LSA lithics associated with the geological samples described above. Few to no vertebrate fossils have been found associated with the abundant evidence of flaked and ground stone technology belonging to the LSA technocomplex (*SI Appendix*, Figs. S17–S19). Obsidian is the single dominant raw material type, with siliceous rocks represented by only a few pieces. Blades dominate the assemblages, but bladelets and convergent and oval-shaped flakes are also present. Sizes of flakes and blades are generally much larger than the younger OUD LSA assemblage (below). Crested blades attest to being removed sequentially from prismatic/pyramidal cores, and some blades and Levallois products were retouched into end scrapers and points. Ground stone implements include hand stones and fragments of lower grindstones.

Messalou's OUD LSA. The OUD area east of the modern Awash River (Fig. 1) contains a set of LSA occupations whose importance was recognized in the mid-1970s (21). Additional reconnaissance, excavation, and sampling of Locality OUD-A1 in 2018 led to the establishment of a local measured section (Fig. 2) that includes two tuffs and archaeological remains, including OES and a variety of flaked and ground stone tools attributable to the LSA.

The OUD beds comprise interbedded fluvial and lacustrine basin-fill tuffaceous sediments deposited unconformably upon eroded Pliocene basement rocks. These filled the base of a small basin created by basalts forming the Namey Koma volcanic edifice in the uppermost catchment of the Messalou drainage east of the modern Awash (Fig. 1). The LSA-bearing light brownish gray tuffaceous silty clay beds are massive, variably consolidated, and represent laterally continuous, gently sloping erosional surfaces with abundant artifacts, unlike the ledge-forming, reworked tuff and unconsolidated gray silt below. The uppermost light brown silty clay contains no stone tools.

The tuffaceous lake margin sediments bearing densely concentrated LSA artifacts at OUD-A1 are intercalated with two unconsolidated, laterally discontinuous, fine- to coarse-grained reworked vitric tuffs (MA18-11 and 18-13; Fig. 2). These tuffs are ∼30 cm thick and separated by ∼1.7 m. Our hypothesis that these might correlate with the two Wallia beds tephra described above was falsified by laboratory analysis showing the glass components to be compositionally distinct and preserving abbreviated linear compositional arrays (*SI Appendix*, Table S2 and Figs. S21 and S22). MA18-13 is also multimodal, preserving a minor mode compositionally equivalent to the underlying MA18-11 tuff, indicating incorporation of MA18-11 shards during deposition/reworking (Dataset S1).

OES fragments from the archaeologically rich silty clay layer were surface-collected and ^{14}C-dated to between 23.9 to 21.4 cal ka BP, thus ∼10 ka younger than the Wallia LSA (Fig. 3 and Dataset S1).

We intensively surveyed and then performed DGPS-controlled collection of diagnostic surface artifacts at OUD-A1, followed by a 35-m^2 excavation. Bone was absent from both, but OES was well-preserved. Lithic raw material quality and diversity are high, including silicious rocks, obsidian, and fine-grained basalt extracted from cobbles and boulders exposed in adjacent slopes of older basement sediments. The assemblage is microlith-dominated. Assemblage analysis is currently underway, but field observations allow introductory characterization of the assemblage (*SI Appendix*, Figs. S18 and S19).

Cores are mostly single- (and less commonly opposed-) platform, usually pyramidal, and less frequently prismatic. Most flakes are laminar, in the bladelet category. Platform preparation was by core-tablet removals usually on elongate pebbles/nodules/blocks/blanks that are locally available in the adjacent basement sediments. Simple (unretouched) microliths were the primary targets, although some abrupt backing was applied. True geometric forms are absent, but perforators are present. Ground stone artifacts include hand stones and lower grindstones, the latter mostly fragmentary. The presence of OES beads and preforms among both surface-exposed and excavated materials indicate the local manufacture of these items.

Discussion

Establishment of the chronostratigraphic framework presented here is of pivotal importance because accurate and precise temporal placement is foundational to solving many research questions involving the origin and evolution of African *H. sapiens*. The production of such knowledge will require the effective and precise coupling of recently acquired lake sediment cores with both adjacent and distant geological, archaeological, and paleontological datasets (20).

The Halibee member's sedimentary record contains paleoanthropological resources emplaced episodically within a single depository over ∼200 ka. Its dense and laterally extensive MSA and LSA archaeology and associated faunal occurrences are now emerging across large outcrops that allow sampling of biological and cultural landscapes at ages and scales rarely represented even in eastern Africa. The open-air conditions under which these remains were deposited are distinct from many contemporaneous occurrences recorded in caves or rock shelters.

In situ collections of archaeological and fossil material are valuable for research questions that require high-precision spatial and microstratigraphic data. However, such precise and accurate placements from limited excavations into large open-air occurrences often generate inadequate samples with which to test various hypotheses about evolution, innovation, and adaptations (17). This is where exploration followed with controlled surface collection of specimens "in stratigraphic context" is a valuable approach (see ref. 45).

For example, by combining surface transects at broad scale, surface collection of assemblages at different spatial and stratigraphic resolutions, and then targeted excavations, our initial findings in the OUD beds illustrate the power of this strategy. There, the remarkable coherence of independently dated samples from a single actively deflating stratum provides a precise age constraint on a substantial collection of artifacts. The LSA there is now firmly placed chrono-stratigraphically and can be characterized typo-technologically. However, understanding the geological and ecological contexts in which this assemblage of artifacts or others like it accumulated is crucial. It is here that the utility of actualistic data becomes apparent.

Fluvial processes and fluviatile ecologies associated with the modern Awash River provide important frameworks for interpreting Halibee's Pleistocene sediments, flora, and fauna (46). For example, recurrent deposition of primarily silty sediments embedding the stratigraphically restricted fossil and artifact

occurrences atop cemented, topographically undulating cobble and pebble conglomerates of the Halibee member indicates seasonal overbank fluvial sedimentation initiated by a relatively elevated base level. Inverted channels with flow directions similar to modern drainage at Halibee further reveal the Pleistocene landscapes during LSA and MSA times.

The Faro Daba beds provide additional evidence from which the MSA landscape may be inferred. Abundant rhizoliths and burned tree root/trunk systems in silty overbank sediments indicate water sufficient to support dense vegetation in proximity to the paleo-Awash and its tributaries here ~100 ka. The cemented underlying DMCC cobble conglomerate would have impeded drainage after seasonal flooding, creating shrinking seasonal ponds flanking the paleo-Awash River and attracting a wide variety of fauna. Modern analogs are observed in the modern Awash River's annual flood cycle.

Pleistocene and Holocene wadi paleochannels now emergent as sinuous inverted sands and pebbles across the Halibee succession represent tributaries that once drained the catchment west of the Halibee area depository, as they do today. These wadis would have provided humans and fauna solid footing and therefore natural corridors to ephemeral ponds and marshes, and thereby to more permanent water, shade, lithic raw material, and biotic resources of the larger paleo-Awash river to the immediate east.

After the richly fossiliferous and artifact-bearing Pleistocene Halibee bed silts representing the seasonally flooded paleolandscape were deposited, these tributary channels—both active as well as inverted—were eventually submerged by progressive sedimentation in expanding seasonal swamps and marshes, with annual sedimentation leveling the topography. The sterility of the overlying finer dark brown clay-rich deposits indicates that the underlying fossil-rich silts were deposited during temporal windows that were relatively short-lived compared to the span of the Halibee member. We predict that continued integration of actualistic investigations in the Middle Awash with the geological and paleobiological evidence from archaeological occurrences will generate multiple testable hypotheses about Pleistocene occupation of the Halibee area.

Broader Implications and Potentials

The paleoanthropological resources of the Afar introduced and calibrated above join a growing body of multidisciplinary evidence with which to investigate current issues in human evolution. For example, there are serious ongoing debates among paleolithic archaeologists about the reality of purported transitions between named archaeological technocomplexes such as the Acheulean, MSA, and LSA (47–50). Indeed, from eastern to western Africa, understanding the nature of the relationship between the MSA and LSA remains incomplete, with little consensus on issues ranging from timing to geography to technology. Understanding the temporal and spatial variation in technologies (51–53), subsistence (54), mobility (55, 56), and potential ecosystem modifications (57) of Middle and Late Pleistocene human populations is best accomplished via comprehensive research on stratified, calibrated sequences of time-successive, geographically limited archaeological occurrences associated with skeletal remains. The rapidly expanding nexus of MSA localities in the Afar thereby creates additional opportunities for progress in testing the modes and tempos of biological and cultural change and the causes of observed variation (58–61).

In the biological realm, the last several decades have witnessed persistent efforts to match oceanic and lacustrine proxies of global climate change with evolutionary events. Many earlier efforts ignored at least some of six fundamental problems involved in any such enterprise practiced at incompatible scales, with deficient datasets, and falsely equating correlation as causation (62). A recent contribution entitled "Rethinking the ecological drivers of hominin evolution" (20) rereviewed these attendant problems and called for a "new phase of paleoanthropological research" (p. 797) that abandons the "pattern matching paradigm" (p. 797) in favor of placing greater emphasis on "theory-driven prediction" (p. 803). Such meta-analyses have their value in paleoanthropology, but they will never substitute for the rare assemblages that combine high ecological and behavioral integrity with negligible time-averaging.

The recent acquisition of calibrated, high-resolution terrestrial lake sediments recording environmental variables has already enhanced knowledge of climate change and attendant complexities of tectonism in eastern Africa (63–66). However, revealing how these dynamics relate to the evolution, dispersal, and behaviors of *H. sapiens* through time requires more than drill cores and will increasingly depend on outcrops of evidence-bearing sediments that accumulated more episodically and whose contents require sustained extraction, comprehensive analysis, and secure age calibration. The Halibee member occurrences described above meet these strict criteria.

Conclusions

The African MSA witnessed the emergence of anatomically modern humans and their expansions to Eurasia (66). Understanding the biology of these people and their descendants requires chronologically placed fossils. Ethiopia now contains a succession of five dated sets of human skeletal remains in MSA contexts: the Omo I partial skeleton at >212 ka (67) and four sets of remains from the Middle Awash: The Chai Baro fossils at >158 ka (see above), the Herto fossils at ~156 to 160 ka (10), the Faro Daba fossils at ~100 ka (see above), and the upper Aduma fossils at <100 ka (3). We anticipate that LSA-associated human remains will follow.

The relative and chronometric placements established above for the sequence of occupations in the Halibee area combine with the high ecological and archaeological integrity of these assemblages to establish the study area's potential for advancing paleoanthropological knowledge of technological, geological, biological, and environmental changes in a single basin during a period widely associated with the ultimate emergence and dispersal of modern humans.

A recent summary (66) concluded that "interdisciplinary analysis … will undoubtedly reveal new surprises about the roots of modern human ancestry." (p. 235). The Halibee member's contributions to understanding the anatomical, behavioral, and ecological aspects of this ancestry are evident. Establishment of a sound chronostratigraphic framework via independent, cross-verifying chronometers is foundational to ongoing paleoanthropological research. Our results demonstrate the power of sustained field and laboratory work and further confirm that the deep sedimentary stack of Ethiopia's Afar remains central to understanding the origins and evolution of our species.

Methods

Field and laboratory methods employed to generate the results described above are standard in geoscience and paleoanthropology. Detailed descriptions and illustrations of these methods are presented in *SI Appendix*.

Data Availability. All study data are included in the article and/or supporting information.

ACKNOWLEDGMENTS. We thank the dozens of Ph.D.-level scientists and support staff conducting field and laboratory research in the Middle Awash since 1981 (full listing at https://middleawash.berkeley.edu/). We thank the Authority for Research and Conservation of the Cultural Heritage and the National Museum of Ethiopia, the Afar Regional Government, and the Afar people of the Middle Awash, as well as the many others who contributed directly to the research efforts and results since 1981. Support from the John Templeton

Foundation is gratefully acknowledged. This work was further supported in part by the Institute of Geophysics and Planetary Physics of the Los Alamos National Laboratory, Digital Globe, the Japan Society for the Promotion of Science, and donors to the Human Evolution Research Center. E.M.N. and W.D.S. were supported by NSF Grant BCS-1727085 to W.D.S. and C.A. Tryon and by the Ann and Gordon Getty Foundation, with thanks to Christina Polito-Halter and Brian Jones for help with ^{230}Th/U analyses and Luis-Erick Aguirre Palafox and Chihiro Ishida for geochronological sample preparation assistance. W.K.H. acknowledges support from the Janet and Elliot Baines Professorship at Miami University (2010-15); M.F.B. acknowledges support from the University of California, Berkeley Chancellor's Fellowship and University of California, Berkeley Portuguese Studies Program; Y.S. and Y.B. acknowledge support from the L.S.B. Leakey Foundation and the Paleontological Scientific Trust for archaeological fieldwork and laboratory analyses, including obsidian geochemistry. Any opinions, findings, and conclusions expressed in this study are those of the authors and do not necessarily reflect the views of the granting agencies or institutions named above.

1. F. E. Grine, "The late Quaternary hominins of Africa: The skeletal evidence from MIS 6-2" in *Africa from MIS 6-2: Population Dynamics and Paleoenvironments*, S. C. Jones, B. A. Stewart, Eds. (Springer, Dordrecht, 2016), pp. 403–420.
2. S. H. Ambrose, "Chronological calibration of Late Pleistocene modern human dispersals, climate change and archaeology with geochemical isochrons" in *Modern Human Origins and Dispersal*, Y. Sahle, H. Reyes-Centeno, C. Bentz, Eds. (Kerns Verlag, Tübingen, 2019), pp. 171–213.
3. J. E. Yellen *et al.*, The archaeology of Aduma Middle Stone Age sites in the Awash Valley, Ethiopia. *PaleoAnthropology* **10**, 25–100 (2005).
4. T. Devièse *et al.*, Direct dating of Neanderthal remains from the site of Vindija Cave and implications for the Middle to Upper Paleolithic transition. *Proc. Natl. Acad. Sci. U.S.A.* **114**, 10606–10611 (2017).
5. T. Devièse *et al.*, Reevaluating the timing of Neanderthal disappearance in Northwest Europe. *Proc. Natl. Acad. Sci. U.S.A.* **118**, e2022466118 (2021).
6. H. Fewlass *et al.*, A ^{14}C chronology for the Middle to Upper Palaeolithic transition at Bacho Kiro Cave, Bulgaria. *Nat. Ecol. Evol.* **4**, 794–801 (2020).
7. N. Blegen, B. R. Jicha, S. McBrearty, A new tephrochronology for early diverse stone tool technologies and long-distance raw material transport in the Middle to Late Pleistocene Kapthurin Formation, East Africa. *J. Hum. Evol.* **121**, 75–103 (2018).
8. A. L. Deino *et al.*, Chronology of the Acheulean to Middle Stone Age transition in eastern Africa. *Science* **360**, 95–98 (2018).
9. L. E. Morgan, P. R. Renne, Diachronous dawn of Africa's Middle Stone Age: New ^{40}Ar/^{39}Ar ages from the Ethiopian Rift. *Geology* **36**, 967–970 (2008).
10. T. D. White *et al.*, Pleistocene *Homo sapiens* from Middle Awash, Ethiopia. *Nature* **423**, 742–747 (2003).
11. L. E. Morgan, P. R. Renne, R. E. Taylor, G. WoldeGabriel, Archaeological age constraints from extrusion ages of obsidian: Examples from the Middle Awash, Ethiopia. *Quat. Geochronol.* **4**, 193–203 (2009).
12. K. R. Ludwig, P. R. Renne, Geochronology on the paleoanthropological time scale. *Evol. Anthropol.* **9**, 101–110 (2000).
13. T. M. Smith *et al.*, Earliest evidence of modern human life history in North African early *Homo sapiens*. *Proc. Natl. Acad. Sci. U.S.A.* **104**, 6128–6133 (2007).
14. D. Richter *et al.*, The age of the hominin fossils from Jebel Irhoud, Morocco, and the origins of the Middle Stone Age. *Nature* **546**, 293–296 (2017).
15. I. Hershkovitz *et al.*, The earliest modern humans outside Africa. *Science* **359**, 456–459 (2018).
16. W. D. Sharp, J. B. Paces, Comment on "The earliest modern humans outside Africa". *Science* **362**, 6413 (2018).
17. Y. Sahle *et al.*, "Human emergence: Perspectives from Herto, Afar Rift, Ethiopia" in *Modern Human Origins and Dispersal*, Y. Sahle, H. Reyes-Centeno, C. Bentz, Eds. (Kerns Verlag, Tübingen, 2019), chap. 4, pp. 105–136.
18. L. Spindler *et al.*, Dating the last Middle Palaeolithic of the Crimean Peninsula: New hydroxyproline AMS dates from the site of Kabazi II. *J. Hum. Evol.* **156**, 102996 (2021).
19. W. D. Sharp *et al.*, ^{230}Th/U burial dating of ostrich eggshell. *Quat. Sci. Rev.* **219**, 263–276 (2019).
20. J. T. Faith *et al.*, Rethinking the ecological drivers of hominin evolution. *Trends in Ecol. & Evol.* **36**, 797–807 (2021).
21. J. E. Kalb *et al.*, Fossil mammals and artefacts from the Middle Awash Valley, Ethiopia. *Nature* **298**, 25–29 (1982).
22. J. E. Kalb, C. J. Jolly, E. B. Oswald, P. F. Whitehead, Early hominid habitation in Ethiopia: Recent discoveries of fossils and artifacts in the Middle Awash Valley should yield one of the longest and most complete records of hominid occupation yet described. *Am. Sci.* **72**, 168–178 (1984).
23. W. H. Gilbert, "Introduction" in *Homo erectus: Pleistocene Evidence from the Middle Awash, Ethiopia*, W. H. Gilbert, B. Asfaw, Eds. (University of California Press, 2009), chap. 1, pp. 13–44.
24. J. de Heinzelin, "Geography, mapping, nomenclature" in *The Acheulean and Plio-Pleistocene Deposits of the Middle Awash Valley, Ethiopia*, J. de Heinzelin, J. D. Clark, K. D. Schick, W. H. Gilbert, Eds. (*Annals Sciences Geologiques*, Royal Museum of Central Africa, 2000), chap. 2, *x***vol. 104**, pp. 5–10.
25. Y. Sahle, A. S. Brooks, Assessment of complex projectiles in the early Late Pleistocene at Aduma, Ethiopia. *PLoS One* **14**, e0216716 (2019).
26. J. D. Clark *et al.*, Palaeoanthropological discoveries in the Middle Awash Valley, Ethiopia. *Nature* **307**, 423–428 (1984).
27. P. U. Clark *et al.*, The Last Glacial Maximum. *Science* **325**, 710–714 (2009).
28. E. A. Hensel, R. Vogelsang, T. Noack, O. Bubenzer, Stratigraphy and chronology of Sodicho Rockshelter–A new sedimentological record of past environmental changes and human settlement phases in southwestern Ethiopia. *Front. Earth Sci.* **8**, 640 (2020).
29. C. A. Tryon *et al.*, Middle and Later stone age chronology of Kisese II rockshelter (UNESCO World Heritage Kondoa Rock-Art Sites), Tanzania. *PLoS One* **13**, e0192029 (2018).
30. J. Quade *et al.*, The geology of Gona, Afar, Ethiopia. *Geol. Soc. Am. Bull.* **446**, 1–31 (2008).
31. C. J. Campisano, C. S. Feibel, "Depositional environments and stratigraphic summary of the Pliocene Hadar Formation at Hadar, Afar Depression, Ethiopia" in *The Geology of Early Humans in the Horn of Africa*, J. Quade, J. G. Wynn, Eds. (Springer, 2008), pp. 179–201.
32. T. D. White, Managing paleoanthropology's nonrenewable resources: A view from Afar. *C. R. Palevol* **3**, 341–351 (2004).
33. A. S. Zaki, R. Giegengack, Inverted topography in the southeastern part of the Western Desert of Egypt. *J. Afr. Earth Sci.* **121**, 56–61 (2016).
34. R. Giegengack, A. S. Zaki, Inverted topographic features, now submerged beneath the water of Lake Nasser, document a morphostratigraphic sequence of high-amplitude late-Pleistocene climate oscillation in Egyptian Nubia. *J. Afr. Earth Sci.* **136**, 176–187 (2017).
35. K. M. Stack *et al.*, Comparing orbiter and rover image-based mapping of an ancient sedimentary environment, Aeolis Palus, Gale Crater, Mars. *Icarus* **280**, 3–21 (2016).
36. R. M. Williams, R. P. Irwin III, J. R. Zimbelman, Evaluation of paleohydrologic models for terrestrial inverted channels: Implications for application to Martian sinuous ridges. *Geomorphology* **107**, 300–315 (2009).
37. J. G. Wynn *et al.*, "Stratigraphy, depositional environments, and basin structure of the Hadar and Busidima Formations at Dikika, Ethiopia" in *The Geology of Early Humans in the Horn of Africa*, J. Quade, J. G. Wynn, Eds. (Springer, 2008), pp. 87–118.
38. C. J. Campisano, Geological summary of the Busidima Formation (Plio-Pleistocene) at the Hadar paleoanthropological site, Afar Depression, Ethiopia. *J. Hum. Evol.* **62**, 338–352 (2012).
39. L. J. Noorbergen *et al.*, Long-eccentricity regulated climate control on fluvial incision and aggradation in the Palaeocene of north-eastern Montana (USA). *Sedimentology* **67**, 2529–2560 (2020).
40. A. Nutz *et al.*, Plio-Pleistocene sedimentation in West Turkana (Turkana Depression, Kenya, East African rift system): Paleolake fluctuations, paleolandscapes and controlling factors. *Earth Sci. Rev.* **211**, 103415 (2020).
41. L. R. Binford, *Bones: Ancient Men and Modern Myths* (Academic Press, 2014).
42. A. Negash, F. Brown, B. Nash, Varieties and sources of artefactual obsidian in the Middle Stone Age of the Middle Awash, Ethiopia. *Archaeometry* **53**, 661–673 (2011).
43. P. J. Reimer *et al.*, The IntCal20 Northern Hemisphere radiocarbon age calibration curve (0-55 cal kBP). *Radiocarbon* **62**, 725–757 (2020).
44. A. G. Hogg *et al.*, SHCal20 Southern Hemisphere calibration, 0-55,000 years cal BP. *Radiocarbon* **62**, 759–778 (2020).
45. S. Semaw *et al.*, Co-occurrence of Acheulian and Oldowan artifacts with *Homo erectus* cranial fossils from Gona, Afar, Ethiopia. *Sci. Adv.* **6**, eaaw4694 (2020).
46. J. E. Kalb, M. Jaegar, C. J. Jolly, B. Kana, Preliminary geology, paleontology and paleoecology of a Sangoan site at Andalee, Middle Awash Valley, Ethiopia. *J. Archaeol. Sci.* **9**, 349–363 (1982).
47. J. Shea, *Prehistoric Stone Tools of Eastern Africa: A Guide* (Cambridge University Press, 2020).
48. A. J. Key, I. Jarić, D. L. Roberts, Modelling the end of the Acheulean at global and continental levels suggests widespread persistence into the Middle Palaeolithic. *Hum. and Soc. Sci. Comms.* **8**, 1–12 (2021).
49. S. L. Kuhn, *The Evolution of Paleolithic Technologies* (Routledge, 2020).
50. J. C. Thompson *et al.*, Early human impacts and ecosystem reorganization in southern-central Africa. *Sci. Adv.* **7**, eabf9776 (2021).
51. K. Ranhorn, C. A. Tryon, New radiocarbon dates from Nasera Rockshelter (Tanzania): Implications for studying spatial patterns in Late Pleistocene technology. *J. Afr. Archaeol.* **16**, 1–12 (2018).
52. E. E. Spinapolice, "Lithic variability and cultures in the East African Middle Stone Age" in *Culture History and Convergent Evolution*, H. S. Groucutt, Ed. (Springer, 2020), pp. 87–102.
53. J. Blinkhorn, M. Grove, Explanations of variability in Middle Stone Age stone tool assemblage composition and raw material use in Eastern Africa. *Archaeol. Anthropol. Sci.* **13**, 1–18 (2021).
54. F. Masele, P. R. Willoughby, Zooarchaeology of the Middle Stone Age in Magubike rockshelter, Iringa region, Tanzania. *Afr. Archaeol. Rev.* **1**, 1–21 (2021).
55. C. Oppenheimer *et al.*, Risk and reward: Explosive eruptions and obsidian lithic resource at Nabro volcano (Eritrea). *Quat. Sci. Rev.* **226**, 105995 (2019).
56. Y. V. Kuzmin, C. Oppenheimer, C. Renfrew, Global perspectives on obsidian studies in archaeology. *Quat. Int.* **542**, 41–53 (2020).
57. M. Grove, J. Blinkhorn, Testing the integrity of the Middle and Later Stone Age cultural taxonomic division in eastern Africa. *J. Paleolithic Archaeol.* **4**, 1–24 (2021).
58. C. Shipton *et al.*, The Middle to Later Stone Age transition at Panga ya Saidi, in the tropical coastal forest of eastern Africa. *J. Hum. Evol.* **153**, 102954 (2021).

59. C. A. Tryon, J. T. Faith, Variability in the Middle Stone Age of eastern Africa. *Curr. Anthropol.* **54**, S234–S254 (2013).
60. J. C. Thompson *et al.*, Ecological risk, demography and technological complexity in the Late Pleistocene of northern Malawi: Implications for geographical patterning in the Middle Stone Age. *J. Quat. Sci.* **33**, 261–284 (2018).
61. E. M. L. Scerri *et al.*, Continuity of the Middle Stone Age into the Holocene. *Sci. Rep.* **11**, 70 (2021).
62. T. D. White, "The Pliocene omnivores of Africa: Hominids, suids, and global climatic change" in *Paleoclimate and Evolution, with Emphasis on Human Origins*, E. Vrba, G. Denton, T. Partridge, L. Burkle, Eds. (Yale University Press, 1995), pp. 369–384.
63. C. Campisano *et al.*, The hominin sites and Paleolakes drilling project: High-resolution paleoclimate records from the East African rift system and their implications for understanding the environmental context of hominin evolution. *Paleoanthropology*, **2017**, 1–43 (2017).
64. H. F. Lamb *et al.*, 150,000-year palaeoclimate record from northern Ethiopia supports early, multiple dispersals of modern humans from Africa. *Sci. Rep.* **8**, 1–7 (2018).
65. H. M. Roberts *et al.*, Using multiple chronometers to establish a long, directly-dated lacustrine record: Constraining >600,000 years of environmental change at Chew Bahir, Ethiopia. *Quat. Sci. Rev.* **266**, 107025 (2021).
66. A. Bergström, C. Stringer, M. Hajdinjak, E. M. L. Scerri, P. Skoglund, Origins of modern human ancestry. *Nature* **590**, 229–237 (2021).
67. C. Vidal *et al.*, Age of the oldest *Homo sapiens* from eastern Africa. Research Square [Preprint] (2021). https://doi.org/10.21203/rs.3.rs-373661/v1. Accessed 14 October 2021.